Local electronic structure analysis for brownmillerite Ca(Sr)$FeO_{2.5}$ using site-resolved energy-loss near-edge structures

M. Haruta,[a] H. Kurata, K. Matsumoto, S. Inoue, Y. Shimakawa, and S. Isoda
Institute for Chemical Research, Kyoto University, Uji, Kyoto 611-0011, Japan

(Received 6 May 2011; accepted 14 June 2011; published online 3 August 2011)

Oxygen K-edge and Fe $L_{2,3}$-edge electron energy-loss near-edge structures (ELNES) were measured for FeO_6 octahedra and FeO_4 tetrahedra in the brownmillerite Ca(Sr)$FeO_{2.5}$ by focusing an electron probe at individual Fe sites using scanning transmission electron microscopy combined with electron energy-loss spectroscopy. The observed site-resolved oxygen K-ELNES showed different features reflecting the local chemical bonding around the FeO_6 octahedra and FeO_4 tetrahedra. A pre-peak in the O K-edge spectra, which is attributed to a transition to an unoccupied O 2p band hybridized with the Fe-3d band, shows splitting in the spectrum of the FeO_6 octahedral site. Additionally, for the oxygen linking the octahedral and tetrahedral Fe sites in $CaFeO_{2.5}$, charge transfer was found to preferentially occur toward the tetrahedral Fe ions. In the case of $SrFeO_{2.5}$, charge transfer from the oxygen located in the *ac* plane was biased toward the tetrahedral Fe atoms. Based upon an analysis of the pre-peak intensity of the O K-ELNES, it was concluded that bonding between the oxygen and iron atoms at the tetrahedral site was more covalent in character than at the octahedral site. The strong covalent character of the tetrahedral sites would be one of the reasons for distortion in the FeO_6 octahedra in Ca(Sr)$FeO_{2.5}$, as exhibited by an extension along the *b*-axis. © *2011 American Institute of Physics*. [doi:10.1063/1.3610526]

I. INTRODUCTION

Transition metal oxides in strongly correlated electron systems exhibit a variety of physical properties sensitively related to their crystal structures and constituent elements. Since these structurally complex crystals often have some nonequivalent atomic sites in a unit cell, the local electronic structure is different even for the same element. To further understand such materials it is important to examine the local electronic structure at high spatial resolution. In the case of layered crystals, in particular, it is possible to independently analyze the electronic structure from individual nonequivalent sites[1–4] using electron energy-loss spectroscopy (EELS) combined with high-angle annular dark-field scanning transmission electron microscopy (HAADF-STEM)[5–7] incorporating a spherical aberration corrector for the illuminating lens system.[8,9] The brownmillerite structure ($ABO_{2.5}$) is a typical example of a layered structure with anion vacancy ordering and consists of alternate layers of BO_6 octahedra and BO_4 tetrahedra.

In the present research, the differences between the local electronic structures of the FeO_6 octahedra and FeO_4 tetrahedra were investigated in brownmillerite Ca(Sr)$FeO_{2.5}$ by measuring the O K-edge and Fe $L_{2,3}$-edge energy-loss near-edge structure (ELNES) using the site-resolved scanning transmission electron microscopy combined with electron energy-loss spectroscopy (STEM-EELS) method. The crystal structures of Ca(Sr)$FeO_{2.5}$ have orthorhombic lattice constants of $a = 5.5946$ Å, $b = 14.8273$ Å, and $c = 5.4307$ Å for $CaFeO_{2.5}$,[10] and $a = 5.6685$ Å, $b = 15.5823$ Å, and $c = 5.52653$ Å for $SrFeO_{2.5}$, as determined by powder neutron diffraction analysis and shown schematically in Fig. 1.[11–13] The space groups of $CaFeO_{2.5}$ and $SrFeO_{2.5}$ are *Pcmn* and *Icmm*, respectively. They differ only in the tetrahedral chain ordering. The brownmillerite structure consists of alternate layers of Fe^{3+} O_6 octahedra and Fe^{3+} O_4 tetrahedra along the *b*-axis. They have a G-type antiferromagnetic structure with a spin oriented along the *c*-axis with a high Néel temperature ($T_N = 720$ K for $CaFeO_{2.5}$ and $T_N = 700$ K for $SrFeO_{2.5}$).[14,15] In a G-type structure, the spin directions of near-neighboring Fe^{3+} ions are anti-parallel to each other. In conformity with this magnetic structure, $CaFeO_{2.5}$ has only weak parasitic magnetism along the *a*-axis.[15] The origin of the weak ferromagnetism is considered to be the Dzyalonshinskii-Moriya interaction.[16,17] The magnetic properties of $CaFeO_{2.5}$ are described in terms of superexchange interactions and distortions in the crystal structure.

To better understand the local electronic structure at individual atomic sites, site-resolved EELS offers a promising method which can extract the different local chemical bonding and crystal field splitting around the FeO_6 octahedra and FeO_4 tetrahedra. There are three nonequivalent oxygen atoms and two nonequivalent iron atoms in the unit cell, as shown in Fig. 1. An interesting structural feature is the distortion of the FeO_6 octahedra, in which the Fe1-O2 bond length is longer than the Fe1-O1 bonds in the octahedra. In the case of $CaFe_xMn_{1-x}O_{2.5}$, it was reported that Mn^{3+} preferentially residing in octahedral sites induces a Jahn-Teller distortion.[18] Since Fe^{3+} is a non-Jahn-Teller ion, however, the distortion in the octahedron of Ca(Sr)$FeO_{2.5}$ must arise from other factors. Recently, Grosvenor *et al*. have reported the results of Fe K-edge XANES (x-ray absorption near-

[a]Author to whom correspondence should be addressed. Electronic mail: haruta@eels.kuicr.kyoto-u.ac.jp.

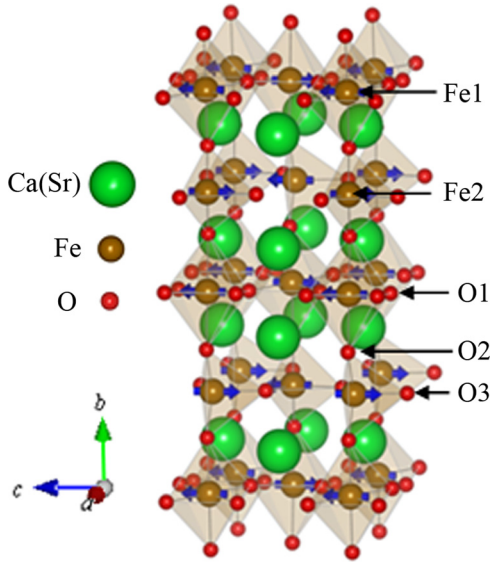

FIG. 1. (Color online) Structure model of brownmillerite $Ca(Sr)FeO_{2.5}$ analyzed by neutron diffraction. There are three nonequivalent oxygen atoms (O1, O2, and O3) in the unit cell. In the G-type magnetic structure, near-neighboring Fe^{3+} ions always have opposite spins.

edge spectroscopy) of $Ca_{2-y}Sr_yFe_2O_5$ and found that as the Sr concentration increases, the unit cell expands, particularly along the *b*-axis, and the degree of O 2p-Fe 4p(3d) orbital overlap decreases.[19] They also discussed the effects of substitution at each site based on the site preference of B-site substitution of ions.[20] The advantage of site-resolved STEM-EELS is the ability to directly examine the nature of the differences at each site. In the present work, we discuss the origins of the distortion by analyzing the site-resolved ELNES using first principles band structure calculations.

II. METHODOLOGY

The brownmillerite $CaFeO_{2.5}$ was prepared by a solid-state stoichiometric reaction of $CaCO_3$ and Fe_2O_3. A mixture of the raw materials was fired at 1200 °C in air for 36 h with intermediate grinding. The STEM samples of $CaFeO_{2.5}$ were prepared by mechanical crushing. A sample of a brownmillerite $SrFeO_{2.5}$ film was fabricated using pulsed laser deposition. The $SrFeO_{2.5}$ thin films were grown heteroepitaxially on $SrTiO_3$ (STO) substrates.[21] The growth temperature was 700 °C in an oxygen partial pressure of 1.0×10^{-5} Torr. Cross-sectional samples were thinned down to electron transparency by ion milling. The thickness of the observed area is about 30 nm, as estimated by EELS measurements. Atomic resolution STEM imaging and EELS measurements were performed at room temperature using a 200 kV TEM/STEM (JEM-9980TKP1; $C_s = -0.025$ mm, $C_5 = 15$ mm) equipped with a spherical aberration corrector for the illuminating lens system. This provided an incident electron probe of less than 0.1 nm in diameter with a convergent semi-angle of approximately 23 mrad. Atomic resolution high-angle annular dark field (HAADF) images were obtained with a detection semi-angle of 70–170 mrad. The EEL spectra were measured using an omega filter with a collection semi-angle of 10 mrad to ensure dipole transition. The energy resolution measured by the full width at half maximum of a zero-loss peak was about 0.5 eV using a cold field emission gun. Additionally, annular bright-field (ABF) imaging was applied to directly observe the distorted FeO_6 octahedra using a JEM-ARM200 F (200 kV, detection angle is about 11.5–23 mrad).[22]

In order to interpret the oxygen K-edge ELNES, first-principles band structure calculations were performed by a full-potential linear augmented plane wave plus local orbital (LAPW + LO) method using the WIEN2k code within the framework of density functional theory.[23] To describe the exchange-correlation potential, spin-polarized generalized-gradient approximation is employed.[24] The values of the atomic sphere radii were chosen as 1.8 a.u. for Ca, 2.2 a.u. for Sr, 1.8 a.u. for Fe, and 1.63 a.u. for O. The ELNES spectra were calculated using the TELNES.2 package incorporated in the WIEN2k code.[25] The effect of a core hole was taken into account in the calculations by introducing a hole in the oxygen 1s state at each nonequivalent oxygen site and adding an electron in the valence band. Calculations including the core-hole were carried out for the primitive unit cell so that the procedure would converge within a practical time. Although the lengths of the *a*- and *c*-axes in the primitive unit cell might not be sufficient to avoid any nonphysical interactions between the core-holes,[26,27] the calculated spectra agreed well with the experimental spectra. Since the structure of $SrFeO_{2.5}$ with the *Icmm* space group includes a randomly-oriented tetrahedral chain within the layer, making it difficult to calculate the band structure, the *Ibm2* space group was also used for $SrFeO_{2.5}$. The crystal orientation effect was not considered in the calculation of the ELNES.

Figure 2(a) shows a typical atomic resolution HAADF image of $SrFeO_{2.5}$ projected along the [101] axis. The Fe columns in the octahedral site appear brighter than those in the tetrahedral site in the HAADF image, which is mainly attributed to electron channeling effects resulting from the different structures along the projection axis.[28] The Fe columns for the tetrahedral iron sites have a dumbbell structure with a small separation, while those for the octahedral iron sites are almost straight columns. In the former columns the probability of electron channeling becomes small, and thus the intensity in the HAADF image is weak compared to that from the

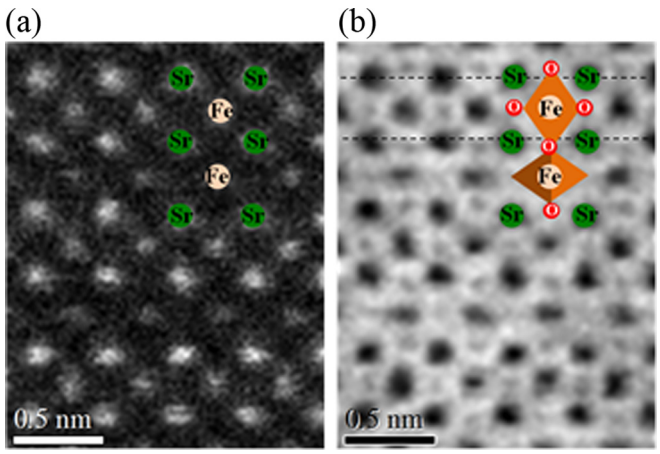

FIG. 2. (Color online) Atomic resolution (a) HAADF and (b) ABF images of $SrFeO_{2.5}$. The oxygen sites can be directly observed in the ABF image, confirming distortion of the FeO_6 octahedra.

latter columns. In order to evaluate the spatial resolution of site-resolved EELS, the delocalization of inelastic scattering due to the excitation of the oxygen 1s electron and the electron channeling effect must be taken into account.[29,30] Since the brownmillerite structure consists of alternate layers of FeO_6 octahedra and FeO_4 tetrahedra along the *b*-axis, it can be expected that specific oxygen atoms coordinating to each Fe site in the unit cell are separately excited when an electron probe is scanned along the same Fe-polyhedral layer (*c*-axis) as described in our previous work.[4]

III. RESULTS AND DISCUSSION

Figure 3 shows experimental site-resolved O K-edge ELNES spectra acquired by scanning an electron probe only at an FeO_6 octahedral site or an FeO_4 tetrahedral site as along with the average spectra obtained by scanning over the whole unit cell of $Ca(Sr)FeO_{2.5}$ for comparison. The calculated spectra including the core-hole are also shown by broken red lines in Fig. 3, and show good agreement with the experimental spectra (solid blue lines). The intensity of the spectra was normalized at about 50 eV far from the edge. The theoretical threshold energy was evaluated by the difference in total energy between the ground state and excited state including the core-hole, and was used to calibrate the difference in threshold energy for each excited O atom. The experimental and calculated spectra were aligned at the threshold. These spectra exhibit different shapes reflecting the local electronic structure around each iron site, although the spectral features of the $CaFeO_{2.5}$ and $SrFeO_{2.5}$ spectra are basically similar. Since the O2 oxygen atoms linking each octahedron and tetrahedron contribute to the experimental spectra at both sites owing to the delocalization of inelastic scattering,[30] each calculated site-resolved spectrum includes contributions from all oxygen atoms forming the octahedra and tetrahedra by taking into account the number of sites contained in the unit cell as described in Ref. 4. By comparing the spectral features with the partial density of states (PDOS), the pre-peak A can be attributed to the transition from the O 1s to the unoccupied O 2p-states hybridized with Fe 3d-states near the Fermi level, while peaks B and C correspond to transitions to the unoccupied O 2p-states mainly hybridized with Ca(Sr) 3d(4d) and Fe 4s/4p states, respectively. Notably, the pre-peak A is significantly different between the octahedral and tetrahedral sites. The pre-peak A in the spectra measured at the octahedral site is split, while that measured at the tetrahedral site is not. This is attributed to the splitting of the Fe 3d band by the crystal field having octahedral or tetrahedral symmetry around each iron site. From a qualitative standpoint, the crystal field splitting at a tetrahedral site is normally smaller than that at an octahedral site for the same ion species. In order to interpret the differences in pre-peak A between the octahedral and tetrahedral sites, we begin by looking at the electronic structure of the ground state in terms of the density of states (DOS) calculated for $CaFeO_{2.5}$, because the band structure can be calculated using the correct space group. Since the experimental ELNES agreed with the spectra calculated for the excited state including the core-hole, the core-hole effect on the unoccupied DOS will be discussed later.

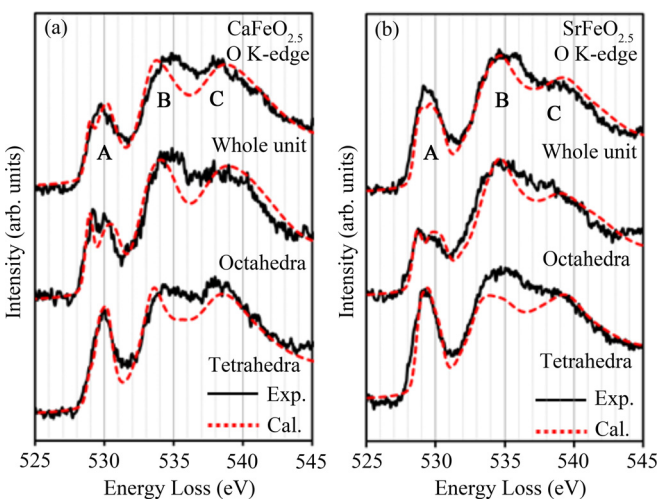

FIG. 3. (Color online) Experimental (blue solid line) and calculated (red dotted line) O K-edge ELNES of (a) $CaFeO_{2.5}$ and (b) $SrFeO_{2.5}$ measured over the whole unit cell, and at the individual FeO_6 octahedral and FeO_4 tetrahedral sites.

Figure 4 shows the spin-polarized Fe 3d-DOS and O 2p-DOS of the ground state projected on the octahedral and tetrahedral atomic sites. Since the Fe^{3+} ion nominally has five d-electrons, half of the 3d-band of Fe site is occupied with electrons having the same spin. If the 3d-band at the Fe1 octahedral site is assumed to be occupied with up-spin electrons, then the Fe2 tetrahedral site must be occupied with down-spin electrons in accordance with the antiferromagnetic structure of type-G, as shown in Fig. 5(a). In that case, the unoccupied 3d-DOS of the Fe1 site has a strong intensity in the down-spin band [Fig. 4(a)], while that of the Fe2 site has a strong intensity in the up-spin band [Fig. 4(b)]. These unoccupied Fe 3d-bands can hybridize with unoccupied O 2p-bands with the same spin of nearest neighbor oxygen ions via superexchange interactions, for instance, between Fe1 and Fe2 ions through an O2 ion. That is, the unoccupied 3d-bands with down-spin at the Fe1 site can hybridize with the unoccupied 2p-bands with down-spin at the O1 and O2 sites. The oxygen 2p-DOS of the down-spin bands at the O1 and O2 sites are shown in Figs. 4 (c) and 4(e), respectively. Conversely, the unoccupied 3d-bands with up-spin at the Fe2 site can hybridize with the unoccupied 2p-bands with up-spin at the O2 and O3 sites [Figs. 4 (e) and 4(d)]. Therefore, the unoccupied 2p-DOS of the O2 site [Fig. 4(e)], linking the Fe1 (octahedral site) and Fe2 ions (tetrahedral site), shows different distributions between the up-spin and down-spin bands, reflecting the different local symmetry around each Fe ion. Similarly, since the O1 ion links two octahedral Fe1 ions having different spin states, unoccupied 2p-bands with up-spin at the O1 site can hybridize with 3d-bands with up-spin at the neighboring Fe ion equivalent with the Fe1 site. The oxygen 2p-DOS of the up-spin bands at the O1 site is similar to that of the down-spin bands [Fig. 4(c)] due to the same local symmetry [Fig. 4(a)].

We note that the Fe 3d-DOS at the Fe1 site clearly splits into three peaks. The first peak, consisting of d_{xy}, d_{yz}, and d_{zx} components, might arise from t_{2g} states, while the e_g states

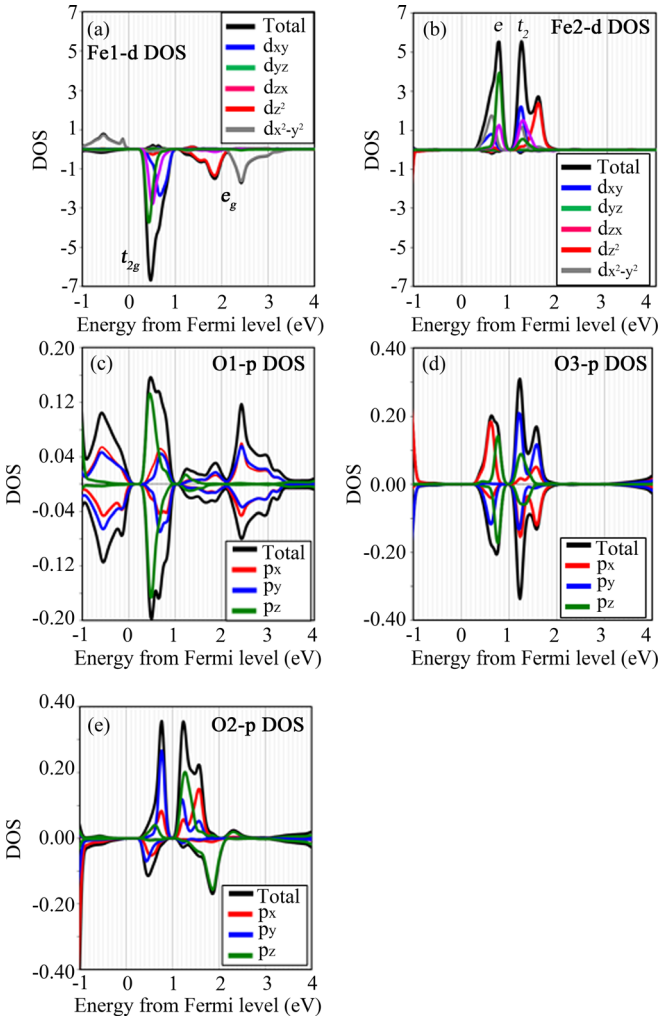

FIG. 4. (Color online) Spin-polarized partial DOS of $CaFeO_{2.5}$ at the ground state. Unoccupied Fe 3d-DOS at (a) the Fe1 octahedral site, and (b) the Fe2 tetrahedral site. Unoccupied O 2p-DOS at (c) the O1 site, (d) the O3 site, and (e) the O2 site.

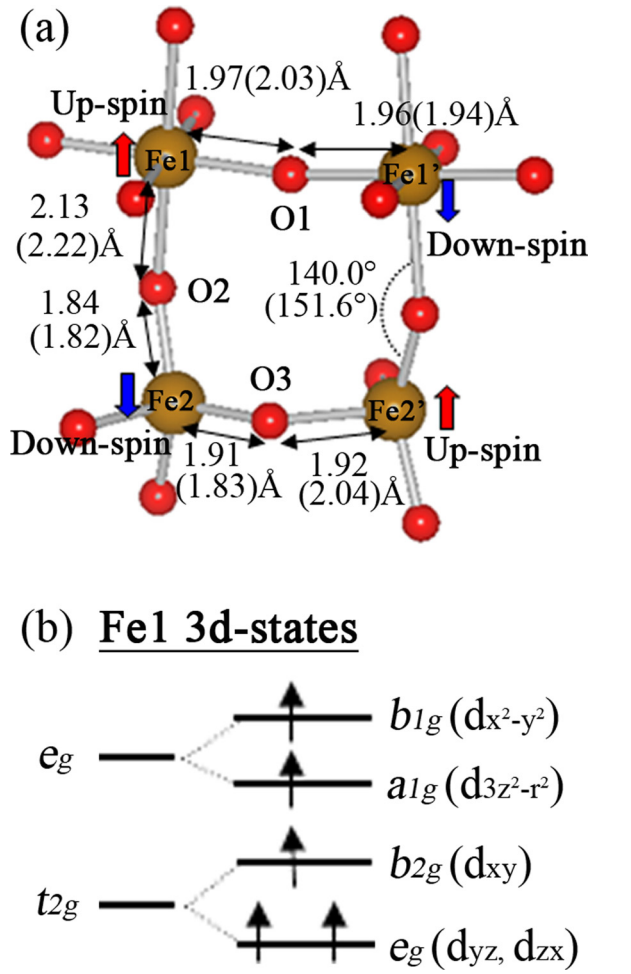

FIG. 5. (Color online) (a) Local structure of FeO_6 and FeO_4 in the Ca(Sr)-$FeO_{2.5}$ crystal. The typical bond lengths and angles are shown. The parenthetic values are for $SrFeO_{2.5}$ with the *Ibm*2 space group. Fe1 at the octahedral site was assumed to be up-spin and Fe2 at the tetrahedral site was assumed to be down-spin. (b) Schematic representation of crystal-field splitting of the Fe1 3d states due to the distortion of the FeO_6 octahedron.

individually split into d_{z^2} and $d_{x^2-y^2}$, which is attributed to distortion of the FeO_6 octahedron from cubic symmetry (O_h) by the periodical ordered oxygen vacancy as shown in Fig. 5(a). Neutron diffraction analysis confirmed that the bond length of Fe1-O2 is longer than that of Fe1-O1.[10] Such a distortion can be directly observed in the ABF image of $SrFeO_{2.5}$ in Fig. 2(b) as a slight, but clear, shift in the oxygen atoms. The distorted crystal field leads to the further splitting of the t_{2g} and e_g states as shown in Fig. 5(b), although Fe^{3+} is not a Jahn-Teller ion. Each oxygen 2p state hybridizes with the Fe 3d state in accordance with the spatial distribution of the 3d orbital as shown in Figs. 4(c) and 4(e). Since the O1 ions bind only to the Fe1 ion in the *ac* plane, the $2p_x$ and $2p_y$ states at O1 strongly hybridize with the $d_{x^2-y^2}$ and d_{xy} states of the Fe1 ion, and the $2p_z$ strongly hybridizes with the d_{yz} and d_{zx} states. However, in the case of the unoccupied down-spin 2p band of the O2 ion, which hybridizes only with the Fe1 octahedral site, the $2p_z$ state strongly hybridizes with d_{z^2}, and there is no hybridization between the O2 2p states and the Fe1 $d_{x^2-y^2}$ state. On the other hand, for the Fe2 ion at the tetrahedral site, the 3d-DOS of Fe2 differs from that of Fe1, reflecting different crystal field splitting (e and t_2) [Fig. 4(b)]. The crystal field splitting at the tetrahedral site is smaller than that at the octahedral site. Since O3 binds only to Fe2 in the *ac* plane, the $2p_x$ and $2p_y$ states strongly hybridize with the d_{xy} or $d_{x^2-y^2}$ state. Furthermore, it should be noted that the unoccupied up-spin $2p_z$ band at the O2 site [Fig. 4(e)] strongly hybridizes with the d_{yz} and d_{zx} states of the Fe2 ion, while the O2 $2p_y$ band hybridizes with the d_{z^2} state because of the large bond angle of Fe1-O2-Fe2 (140.0°).

So far, we have discussed the electronic structure in the ground state. When a core electron is excited to unoccupied states, a hole is generated in the core state. Generally, the core-hole potential modifies the distribution of the DOS at the bottom of the unoccupied band, which is reflected in the observed ELNES. Figures 6(a) and 6(c) show the unoccupied 3d-DOS with down-spin at the octahedral Fe1 site and the unoccupied 2p-DOS with down-spin at the O2 site, respectively, when the 1s electron of the O2 site is excited. On the other hand, when a core-hole exists in the 1s state of O1, each unoccupied DOS projected to the Fe1 and O1 sites is modified differently, as shown in Figs. 6(b) and 6(d). As an overall trend of the core-hole effect, the DOS mainly shifts toward the Fermi level. It should be noted from Figs. 6(a)

and 6(b) that the unoccupied 3d-DOS of the Fe1 site differs depending on the location of the core-hole. In particular, the d_{z^2}, d_{yz}, and d_{zx} states of Fe1 are strongly affected by the introduction of the core-hole at the O2 site as shown in Fig. 6(a), whereas the $d_{x^2-y^2}$ and d_{xy} states of Fe1 are strongly affected by the introduction of the core-hole at the O1 site [Fig. 6(b)]. These changes in the 3d-states of the Fe1 site result from the different screening of the core-hole potential at each O site through hybridization with the oxygen 2p states [Figs. 6(c) and 6(d)]. However, the crystal field splitting of the octahedral site preserves the same features as that of the ground state [Fig. 4(a)]. In the case of the tetrahedral site, the changes in the 3d-DOS of the Fe2 site also depend on the location of the core-hole. Since the ELNES include the core-hole effect, and the O2 linking the octahedral and tetrahedral sites contributes to both experimental site-resolved spectra, interpretation of the experimental spectra is complicated.

The site-resolved ELNES were calculated by using the PDOS including a core-hole at each oxygen site. Figure 7 shows the individual spin-polarized O K-edge ELNES calculated for each oxygen site with a core-hole. The site-resolved ELNES simulated by using these spectra agree well with the experimental spectra as shown in Fig. 3. The peaks A1, A2, and A3 (blue line) in the pre-peak can be attributed to the transition to the O 2p band mainly hybridized with the Fe1$-e_g/b_{2g}$, $-b_{1g}$ and $-a_{1g}$ states, respectively, reflecting the distribution of the Fe-3d orbital in the octahedral site, as mentioned in the preceding text, for Fig. 6. It is concluded that the pre-peak splitting of the experimental spectra at the octahedral site reflects the local electronic structure of the Fe-3d band around the distorted FeO_6 through hybridization between the O 2p and Fe 3d bands. The crystal field splitting at the FeO_4 site is smaller than that at the FeO_6 site [Fig. 3(a)]. These features were also apparent in the case of $SrFeO_{2.5}$.

Since the pre-peak intensity can be correlated to the number of holes at the oxygen site,[31,32] it is worthwhile to investigate this feature in relation to the specific nature of the site and compound. In the case of a purely ionic model, the oxygen 2p states are completely filled, so the channel of transition from the 1s to 2p states in oxygen would be closed in ELNES. However, including some covalent character reduces the number of filled states with oxygen 2p character, and thus, some pre-peak intensity should appear. Since the pre-

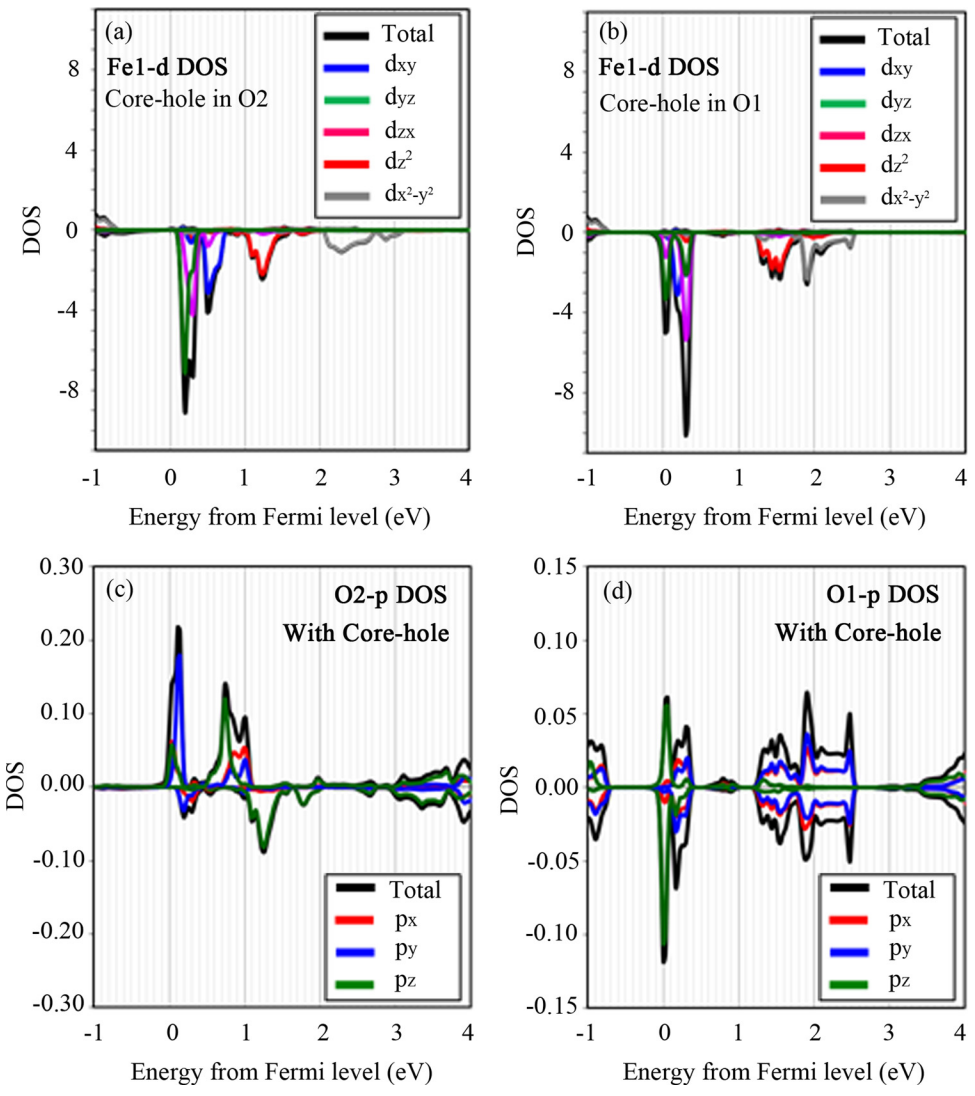

FIG. 6. (Color online) The change in unoccupied spin-polarized DOS of the FeO_6 octahedral site in $CaFeO_{2.5}$ by the core-hole effect. (a) Fe1 3d DOS, and (c) O2 2p DOS when a core-hole exists at the O2 site. (b) Fe1 3d DOS, and (d) O1 2p DOS when a core-hole exists at the O1 site.

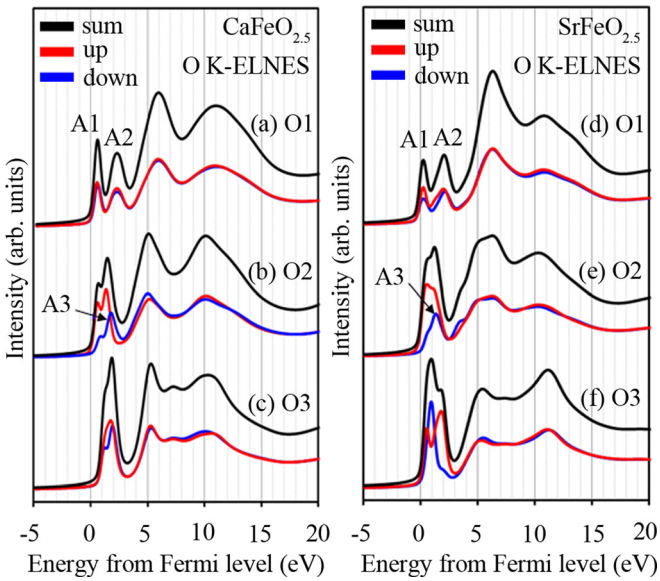

FIG. 7. (Color online) The individual spin-polarized O K-edge ELNES of (a)–(c) $CaFeO_{2.5}$ and (d)–(f) $SrFeO_{2.5}$ calculated for each oxygen site with a core-hole.

peaks are observed in both site-resolved spectra, the chemical bonding around the octahedral and tetrahedral sites clearly has some covalent character. From the Mössbauer spectrum of $CaFeO_{2.5}$, it has been reported that the Fe ions at both sites exist in trivalent states.[33] Therefore, each pre-peak should have the same integrated intensity and, in fact, the site-resolved spectra of $CaFeO_{2.5}$ show almost the same integrated pre-peak intensity between the octahedral and tetrahedral sites [Fig. 3(a)]. In the calculated spectra, however, the pre-peak intensity is different at each oxygen site as shown in Figs. 7(a)–7(c). It can be seen that the pre-peak in the O2 spectrum is slightly smaller than those in the O1 and O3 spectra. Furthermore, the integrated intensity of the pre-peak in the up-spin O2 spectrum [red line in Fig. 7 (b)] is considerably larger than that in the down-spin spectrum [blue line in Fig. 7(b)]. This indicates that the number of holes in the O2 2p band hybridizing with the 3d band of the tetrahedral Fe2 site is greater than that in the O2 2p band hybridizing with the 3d band of the octahedral Fe1 site. This calculated result indicates that charge transfer from O2 to Fe2 is larger than that from O2 to Fe1. Of course, charge transfer also occurs from O3 to Fe2 and from O1 to Fe1, showing the covalent character of the bonding between these atoms, because of the existence of the pre-peaks in the O1 and O3 spectra. However, the asymmetrical charge transfer from O2 to Fe1 and Fe2 should affect the local structure. Specifically, an increase in the covalent character of Fe2-O2 should lead to a decrease in the bond length between Fe2 and O2. In fact, the bond length between Fe2 and O2 at the tetrahedral site (1.84 Å) is shorter than that between Fe1 and O2 at the octahedral site (2.13 Å), as shown in Fig. 5(a). On the other hand, the small pre-peak in the down-spin spectrum of the O2 spectra [blue line in Fig. 7(b)] indicates that a large ionic character exists in the bonding between Fe1 and O2. Since the spin state is not experimentally discriminated and the site-resolved spectra equally detect the contributions from O2 due to the delocalization of inelastic scattering, the spectra measured from the octahedral and tetrahedral sites show almost the same integrated pre-peak intensity. However, the calculations suggest that different amounts of valence charge are localized at the Fe1 and Fe2 ions, which might be detected in the Fe-$L_{2,3}$ edge excitation spectra.

Figure 8 shows the site-resolved Fe $L_{2,3}$-edge spectra of $CaFeO_{2.5}$. The Fe $L_{2,3}$-edge ELNES spectra acquired from the Fe1 octahedral site is similar to a typical Fe^{3+} spectrum measured from hematite, which shows a shoulder peak at the low energy side of the L_3 peak.[20] The L_3 peak of the Fe1 octahedral site is higher in energy by about 0.5 eV than that of the Fe2 tetrahedral site. A similar result has been reported for Fe L_3-edge XANES of $Ca_2Fe_xMn_{1-x}O_5$ (Mn atoms favor occupying the octahedral site).[20] The present result indicates that the transition energy from the Fe 2p level to the Fe 3d-band is lowered at the Fe2 tetrahedral site by the increase in Coulomb repulsion between the 2p electrons and valence electrons due to charge transfer from O2. The chemical shifts in the Fe L_3 peaks at the site-resolved Fe $L_{2,3}$-edge are therefore evidence of charge transfer at the Fe2 tetrahedral site mainly originating from O2. Therefore, it would be considered that the stronger covalent character between O2 and Fe2 at the tetrahedral site arising from the biased charge transfer from O2 to Fe2 contributes heavily to the distortion in the FeO_6 octahedron, although the cause of the distortion in such a complex compound is related to many factors.

On the contrary, in the case of $SrFeO_{2.5}$, the integrated intensity of the pre-peak A from the FeO_4 tetrahedral site was obviously larger than that from the FeO_6 octahedral site in both the experimental and calculated spectra as shown in Fig. 3(b). This result suggests that the pre-peak intensity in the O1 spectrum might differ from that in the O3 spectrum. In fact, the integrated intensity of the pre-peaks in both the O2 and O3 spectra are considerably larger than that in the

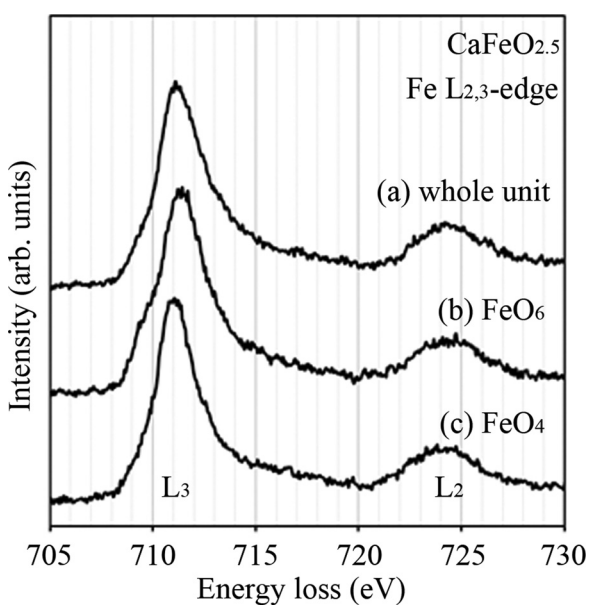

FIG. 8. Experimental Fe $L_{2,3}$-edge ELNES of $CaFeO_{2.5}$ for (a) the whole unit cell, and at the (b) FeO_6 octahedral. and (c) FeO_4 tetrahedral sites, respectively.

O1 spectrum, as shown in the calculated spectra of Figs. 7(d)–7(f). These results indicate that the tetrahedral site of $SrFeO_{2.5}$ has a strong covalent character in comparison to that of $CaFeO_{2.5}$. The substitution from Ca to Sr leads to an increase in the bond length between Fe1 and O2 compared to other Fe-O bonds, while the Fe2-O2 bond is not greatly changed, as shown in Fig. 5(a).[19] However, the integrated intensity of the pre-peak related to the tetrahedral site [red line in Figs. 7(b) and 7(e)] significantly changes compared to that of the octahedral site [blue line in Figs. 7(b) and 7(e)] upon substitution with the Sr ion. As a general trend, since A-site substitution with a larger ion (Ca → Sr) leads to an increase in the bond angle of Fe1-O2-Fe2 (140.0° → 151.6°), it is considered that an increase in overlap between the O2 2p and Fe2 3d orbitals affects the covalent character between these ions in $SrFeO_{2.5}$. On the contrary, it should be noted that the pre-peak intensity in the O3 spectrum varies between the up- and down-spin spectra in $SrFeO_{2.5}$, as shown in Fig. 7(f). The O3 atom links the Fe2 and Fe2′ atoms, having opposite spin as shown in Fig. 5(a). Since the up-spin spectrum is related to bonding with the Fe2 atom, the relatively strong pre-peak of this spectrum indicates a large charge transfer from O3 to Fe2, as compared to that from O3 to Fe2′. Such an asymmetrical charge transfer from O3 to the tetrahedral Fe atoms should lead to the observed difference in bond lengths between Fe2-O3 (1.83 Å) and Fe2′-O3 (2.04 Å). Therefore, the Fe2-O3 bond has a strong covalent character and charge transfer as compared to the Fe2′-O3 bond. The band structure of $SrFeO_{2.5}$ was calculated by assuming the *Ibm2* space group, which predicts an asymmetrical charge transfer from O3 to Fe2. Since the actual space group of $SrFeO_{2.5}$ is *Icmm*, which includes the randomly oriented tetrahedral chain within the layer, it appears that the strong charge transfer from O3 to the Fe2 atoms occurs randomly at either side. Therefore, the *Icmm* space group for $SrFeO_{2.5}$ can be attributed to the random charge transfer from O3 to Fe2 at the FeO_4 tetrahedral site.

IV. CONCLUSIONS

In the present research, O K-edge and Fe $L_{2,3}$-edge ELNES were measured at FeO_6 octahedra and FeO_4 tetrahedra in the brownmillerite $Ca(Sr)FeO_{2.5}$ by focusing an electron probe at each Fe site using STEM-EELS. The observed site-resolved oxygen K-ELNES showed specific features reflecting the local chemical bonding around the FeO_6 octahedra and FeO_4 tetrahedra. The splitting observed in the pre-peak of the O K-edge, indicating transition to an unoccupied O-2p band hybridized with the Fe-3d band, demonstrated the strong crystal field of the octahedral site as compared to the tetrahedral site. The site-resolved O K-ELNES were in fairly good agreement with the calculated spectra based on the unoccupied O 2p-DOS, including a core-hole at each independent oxygen site. From a detailed analysis of the pre-peak intensity of O K-ELNES, it was found that asymmetrical charge transfer occurs at the O2 atom, linking the octahedral and tetrahedral Fe atoms in $Ca(Sr)FeO_{2.5}$. The charge transfer from O2 to the tetrahedral Fe2 atom is larger than that to the octahedral Fe1 atom. This indicates that the bonding character between O2 and the tetrahedral Fe2 atoms is more covalent than that between the O2 and Fe1 atoms, which leads to the observed difference in bond length between O2-Fe2 and O2-Fe1. The FeO_6 octahedra are distorted by an ordered oxygen vacancy, which was directly observed as slight shifts in the O2 atoms at the tetrahedral Fe2 site in the ABF image, reflecting the long bond length of O2-Fe1. Therefore, the stronger covalent character between O2 and Fe2 at the tetrahedral site arising from the biased charge transfer from O2 to Fe2 would be one of the reasons for the distortion in the FeO_6 octahedron. The distortion of the FeO_6 octahedra was clearly observed as a slight shift of apical oxygen columns in the ABF-STEM image.

Asymmetrical charge transfer was also identified at the O3 atom linking the tetrahedral Fe atoms in $SrFeO_{2.5}$. It was concluded that the difference in bond length between O and the various tetrahedral Fe atoms in the *ac* plane was caused by an asymmetrical charge transfer, leading to each O-Fe bond having different covalent character at the tetrahedral site in $SrFeO_{2.5}$.

ACKNOWLEDGMENTS

This work was partly supported by Grants-in-Aid for Scientific Research Grant No.19GS0207 from the Ministry of Education, Culture, Sports, Science, and Technology, Japan. We acknowledge Mr. Kawasaki, Dr. Otsuka, and Miss Nishimura of TRC for preparing the cross-section samples, and Dr. Okunishi of JEOL for the ABF image.

[1]Y. Ito, R. F. Klie, and N. D. Browning, J. Am. Ceram. Soc. **85**(4), 969 (2002).
[2]T. Mizoguchi, M. Varela, J. P. Buban, T. Yamamoto, and Y. Ikuhara, Phys. Rev. B **77**, 024504 (2008).
[3]G. Yang, Q. Ramasse, and R. F. Klie, Phys. Rev. B **78**, 153109 (2008).
[4]M. Haruta, H. Kurata, H. Komatsu, Y. Shimakawa, and S. Isoda, Phys. Rev. B **80**, 165123 (2009).
[5]N. D. Browning, M. F. Chisholm, and S. J. Pennycook, Nature (London) **366**, 143 (1993).
[6]D. A. Muller, T. Sorsch, S. Moccio, F. H. Baumann, K. Evans-Lutterodt, and G. Timp, Nature (London) **399**, 758 (1999).
[7]M. Varela, S. D. Findlay, A. R. Lupini, H. M. Christen, A. Y. Borisevich, N. Dellby, O. L. Krivanek, P. D. Nellist, M. P. Oxley, L. J. Allen, and S. J. Pennycook, Phys. Rev. Lett. **92**, 095502 (2004).
[8]P. E. Batson, N. Dellby, and O. L. Krivanek, Nature (London) **418**, 617 (2002).
[9]P. D. Nellist, M. F. Chisholm, N. Dellby, O. L. Krivanek, M. F. Murfitt, Z. S. Szilagyi, A. R. Lupini, A. Borisevich, W. H. Sides, Jr., and S. J. Pennycook, Science **305**, 1741 (2004).
[10]P. Berastegui, S. G. Eriksson, and S. Hull, Mater. Res. Bull. **34**, 303 (1999).
[11]C. Greaves, A. J. Jacobson, B. C. Tofield, and B. E. F. Fender, Acta Crystallogr., Sect. B: Struct Crystallogr. Cryst. Chem. **31**, 641 (1975).
[12]M. Schmidt, and S. J. Champbell, J. Solid State Chem. **156**, 292 (2001).
[13]H. D'Hondt, A. M. Abakumov, J. Hadermann, A. S. Kalyuzhnaya, M. G. Rozova, E. V. Antipov, and G. V. Tendeloo, Chem. Mater. **20**, 7188 (2008).
[14]T. Takeda, Y. Yamaguchi, H. Watanabe, S. Tomiyoshi, and H. Yamamoto, J. Phys. Soc. Japan **26**, 1320 (1969).
[15]T. Takeda, Y. Yamaguchi, S. Tomiyoshi, M. Fukase, M. Sugimoto, and H. Watanabe, J. Phys. Soc. Japan **24**, 446 (1968).
[16]I. E. Dzyaloshinskii, J. Phys. Chem. Solids **4**, 241 (1958).
[17]T. Moriya, Phys. Rev. **120**, 91 (1960).
[18]F. Remezanipour, B. Cowie, S. Derakhshan, J. E. Greedan, and L. M. D. Cranswick, J. Solid State Chem. **182**, 153 (2009).
[19]A. P. Grosvenor and J. E. Greedan, J. Phys. Chem. C **113**, 11366 (2009).

[20]A. P. Grosvenor, F. Ramezanipour, S. Derakhshan, C. Maunders, G. A. Botton, and J. E. Greedan, J. Mater. Chem. **19**, 9213 (2009).
[21]S. Inoue, M. Kawai, Y. Shimakawa, M. Mizumaki, N. Kawamura, T. Watanabe, Y. Tsujimoto, H. Kageyama, and K. Yoshimura, Appl. Phys. Lett. **92**, 161911 (2008).
[22]S. D. Findlay, N. Shibata, H. Sawada, E. Okunishi, Y. Kondo, T. Yamamoto, and Y. Ikuhara, Appl. Phys. Lett. **95**, 191913 (2009).
[23]P. Blaha, K. Schwarz, G. K. H. Madsen, D. Kvasnicka, and J. Luitz, wien2k, An Augmented Plane Wave + Local Orbitals Program for Calculating Crystal Properties, Vienna University of Technology, Vienna, Austria 2002.
[24]J. P. Perdew, S. Burke, and M. Ernzerhof, Phys. Rev. Lett. **77**, 3865 (1996).
[25]C. Hébert, J. Luitz, and P. Schattschneider, Micron **34**, 219 (2003).
[26]S. D. Mo, and W. Y. Ching, Phys. Rev. B **62**, 7901 (2000).
[27]T. Mizoguchi, I. Tanaka, S. Yohioka, M. Kunisu, T. Yamamoto, and W. Y. Ching, Phys. Rev. B **70**, 045103 (2004).
[28]M. Haruta, H. Kurata, H. Komatsu, Y. Shimakawa, and S. Isoda, Ultramicroscopy **109**, 361 (2009).
[29]M. P. Oxley, M. Varela, T. J. Pennycook, K. van Benthem, S. D. Findlay, A. J. D'Alfonso, L. J. Allen, and S. J. Pennycook, Phys. Rev. B **76**, 064303 (2007).
[30]M. Varela, M. P. Oxley, W. Luo, J. Tao, M. Watanabe, A. R. Lupini, S. T. Pantelides, and S. J. Pennycook, Phys. Rev. B **79**, 085117 (2009).
[31]F. M. F. de Groot, M. Grioni, J. C. Fuggle, J. Ghijsen, G. A. Sawatzky, and H. Petersen, Phys. Rev. B **40**, 5715 (1989).
[32]H. Kurata and C. Colliex, Phys. Rev. B **48**, 2102 (1993).
[33]M. Eibschütz, U. Ganiel, and S. Shtrikman, J. Mater. Sci. **4**, 574 (1969).